A simulation study of a dual-plate in-room PET system for dose verification in carbon ion therapy *

CHEN Ze(陈泽)[1,2] HU Zheng-Guo(胡正国)[1;1)] CHEN Jin-Da(陈金达)[1]
ZHANG Xiu-Ling(张秀玲)[1] GUO Zhong-Yan(郭忠言)[1] XIAO Guo-Qing(肖国青)[1]
SUN Zhi-Yu(孙志宇)[1] HUANG Wen-Xue(黄文学)[1] WANG Jian-Song(王建松)[1]

[1] Institute of Modern Physics, Chinese Academy of Sciences, Lanzhou 730000, China
[2] University of Chinese Academy of Sciences, Beijing 100049, China

Abstract: During carbon ion therapy, lots of positron emitters such as ^{11}C, ^{15}O, ^{10}C are generated in irradiated tissues by nuclear reactions, and can be used to track the carbon beam in the tissue by a positron emission tomography (PET) scanner. In this study, an dual-plate in-room PET scanner has been designed and evaluated based on the GATE simulation platform to monitor patient dose in carbon ion therapy. The dual-plate PET is designed to avoid interference with the carbon beamline and with patient positioning. Its performance was compared with that of four-head and full-ring PET scanners. The dual-plate, four-head and full-ring PET scanners consisted of 30, 60, 60 detector modules, respectively, with a 36 cm distance between directly opposite detector modules for dose deposition measurements. Each detector module consisted of a 24×24 array of 2 mm×2 mm×18 mm LYSO pixels coupled to a Hamamatsu H8500 PMT. To estimate the production yield of positron emitters, a 10 cm×15 cm×15 cm cuboid PMMA phantom was irradiated with 172, 200, 250 MeV/u ^{12}C beams. 3D images of the activity distribution measured by the three types of scanner are produced by an iterative reconstruction algorithm. By comparing the longitudinal profile of positron emitters along the carbon beam path, it is indicated that use of the dual-plate PET scanner is feasible for monitoring the dose distribution in carbon ion therapy.

Key words: hadron therapy, PET, GATE, simulation

PACS: 87.55.de, 87.55.Gh, 87.55.K- **DOI:** 10.1088/1674-1137/38/8/088202

1 Introduction

In tumor treatment, carbon ion therapy has the ability to overcome the limitations of conventional radiotherapy due to most energy deposition being at a selective depth, usually called the Bragg peak, which results in increased biological effectiveness. Since in carbon ion therapy, misalignment of the carbon beam, patient mispositioning or changes in the structure or density of the irradiated tissue may result in dose reduction within the tumor or overdosing in organs at risk [1], the correct depth of the Bragg peak is crucial. Considering the above situation, a tool that can monitor the treatment dose distribution in vivo and non-invasively is required. A positron emission tomography (PET) scanner is a feasible solution for this purpose because it can image the 3D distribution of positron emitters produced by nuclear fragmentation reactions of the projectiles with target nuclei [2, 3].

There are three types of PET scanner [4] (in-beam, in-room, and off-line) which have been confirmed to have the feasibility to monitor the dose deposition in radioactive therapy. Although the in-beam PET measurement is only slightly influenced by metabolic processes and blood flow, additional efforts are required to provide radiation hard components and to suppress the strong γ-ray background from the interactions of the beam and patient. The in-room PET technique is adopted as a compatible trade-off between performance and cost. In order to avoid interference between the PET detectors and the hadron beamline and patient positioning, a dual-plate geometry is chosen.

In this study, we use the GATE [5] simulation platform to evaluate the performance of dual-plate PET, and compare with that of four-head and full-ring PET scanners. The dose distribution of the carbon beam and

Received 9 October 2013

∗ Supported by National Natural Science Foundation of China (11205222), West Light Foundation of the Chinese Academy of Sciences (210340XBO), National Major Scientific Instruments and Equipment Development Projects (2011YQ12009604) and Youth Innovation Promotion Association, CAS (201330YQO)

1) E-mail: huzg@impcas.ac.cn

production yields of the positron emitters were simulated for different carbon beam energies in a cuboid PMMA phantom. 3D images of the activity distribution from the three types of scanner are produced by an iterative reconstruction algorithm, and the longitudinal profile images of positron emitters are compared.

2 Materials and methods

2.1 Description of in-room PET scanner

To avoid interference with the beamline, the in-room PET is based on two plate heads, which are made of 3×5 detector modules, respectively. Each detector module consists of a 24×24 array of 2 mm×2 mm×18 mm LYSO pixels coupled to a Hamamatsu H8500 PMT. In the simulation, we only consider the energy deposition in the LYSO array to simplify the simulation process. Table 1 describes the hadronic physics processes used in the GATE simulation.

Figure 1 shows the configurations of all three simulated PET geometries. The dual-plate, four-head and full-ring PET scanners consist of 30, 60 and 60 detector modules, respectively, with a 36 cm distance between directly opposite detector modules for dose deposition measurements.

Table 1. Hadronic models used in GATE simulation.

hadronic process	particle	Geant4 process	Geant4 model	Geant4 dataset	energy range
elastic scattering	generic ion	G4 hadron elastic process	G4L elastic	G4 hadron elastic dataSet	—
	all other particles	G4 proton inelastic process	G4 hadron elastic	G4 hadron elastic dataSet	—
inelastic process for protons	protons	G4 proton inelastic process	G4 binary cascade	G4 proton inelastic cross section	0–500 GeV
inelastic process for ions	generic ion, deuteron, triton, alpha	G4 ion inelastic process	G4QMD reaction	G4 ions shen cross section	0–500 GeV
inelastic scattering for neutrons	neutron	G4 neutron inelastic process	G4 neutron HP inelastic	G4 neutron HP inelastic data	0–20 MeV
			G4 binary cascade	G4 neutron inelastic cross section	14 MeV–500 GeV

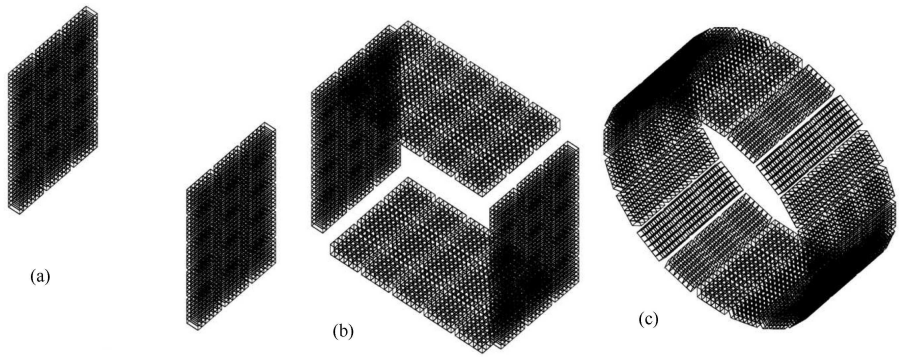

Fig. 1. The simulated PET geometry configuration. (a) dual-plate; (b) four-head; (c) full-ring.

2.2 Performance of in-room PET scanners

Before the radiation therapy simulation, we evaluated the spatial resolution of the reconstructed images of the three kinds of PET scanner. The measurement was carried out by positioning 9 ^{22}Na point sources (0.5 mm diameter) along the X-axis, ranging from −8 to 8 cm with a 2 cm interval between each source. The spatial resolution in the radial and tangential directions was measured by fitting Gaussian functions to the respective profiles of the reconstructed images of the point sources. We use the iterative reconstruction algorithm, which is based on maximum likelihood expectation maximization (MLEM) algorithm, to produce the 3D image of the activity distribution.

2.3 Production yield of positron emitters

GATE V6.2, which provides lots of useful tools to collect information during simulation, is used in this study. We use the "ProductionAndStoppingActor" to estimate the distributions of ^{11}C, ^{15}O, ^{10}C, and "DoseActor" to calculate the dose distributions. In the simulation, the carbon ion beam irradiated a PMMA phantom with dimensions of 10 cm×15 cm×15 cm to estimate the production yield and distribution of positron emitters. The

carbon beam is delivered along the Z-axis to the smallest cross-section (10 cm×15 cm) of the phantom. Three beam energies are selected: 172, 200, 250 MeV/u, based on a typical treatment plan. The beam profile in the transverse direction is assumed to be a Gaussian shape with a FWHM of 8 mm. The intensity of the beam is 1×10^6 pps. Positron emitters such as ^{11}C, ^{15}O, ^{10}C generated in irradiated tissues by nuclear reactions are analyzed.

The phantom images are reconstructed by the MLEM algorithm, and the longitudinal profiles of the reconstructed images are calculated by ROOT software. Last, the dose verification is evaluated by comparing the distribution of the positron emitter from "ProductionAndStoppingActor" and the image profile measured by the PET scanner.

3 Results

3.1 Performance of three kinds of PET scanner

Figure 2 shows the reconstructed images of the point sources at different positions measured by the three PET scanners. With the dual-head, image of the point sources in the near-peripheral region of the field of view (FOV) is blurred, while the four-head and full-ring PET scanners show relatively uniform imaging characteristics over the entire FOV. The radial and tangential spatial resolutions are illustrated in Fig. 3 for different positions along the X-axis across the FOV.

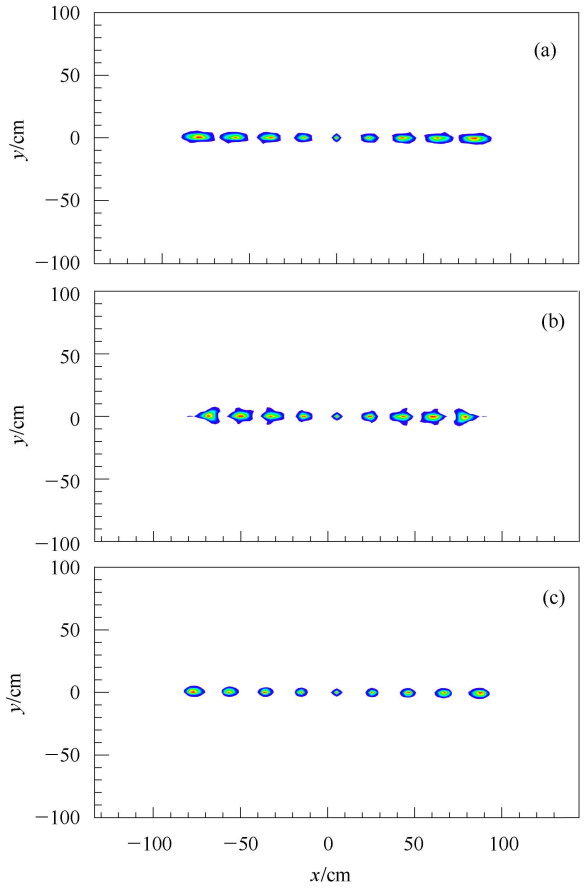

Fig. 2. (color online) The reconstructed images of point sources at different positions. (a) dual-plate; (b) four-head; (c) full-ring.

The sensitivities of the three kinds of PET scanner, measured with a 1.0 MBq ^{22}Na point source, stepped at 2 cm increments in radial direction and with an energy window (350–650 keV), are shown in Fig. 4. The sensitivity of the ring is nearly three times higher than that of the dual-plate.

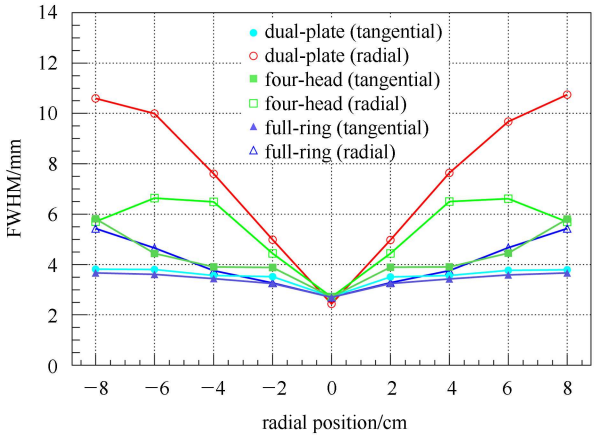

Fig. 3. (color online) Spatial resolution in radial and tangential directions for radial locations in the FOV. Resolutions are based on a 1.0 MBq ^{22}Na point source measured in air and reconstructed with MLEM.

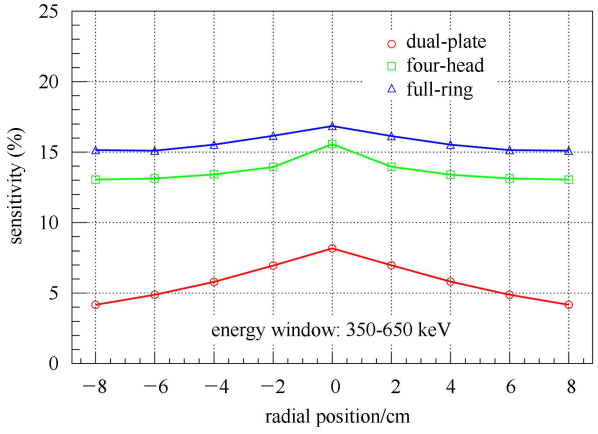

Fig. 4. (color online) The sensitivities of the three kinds of PET scanner.

3.2 Yields and distributions of positron emitters

The yields of ^{11}C, ^{15}O and ^{10}C produced by 172, 200 and 250 MeV/u carbon beams, respectively, in the

PMMA cuboid phantom are simulated, and listed in Table 2. The yield of ^{11}C, which almost dominates the contribution of positron emitters, is 6 times higher than those of ^{15}O and ^{10}C.

Figure 5 shows the spatial distribution of positron emitters with the corresponding depth-dose distribution of carbon beam. The distance to 50% distal falloff of Bragg peak is 56, 72, 106 mm for the 172, 200 and 250 MeV/u carbon beams, respectively, and the relative

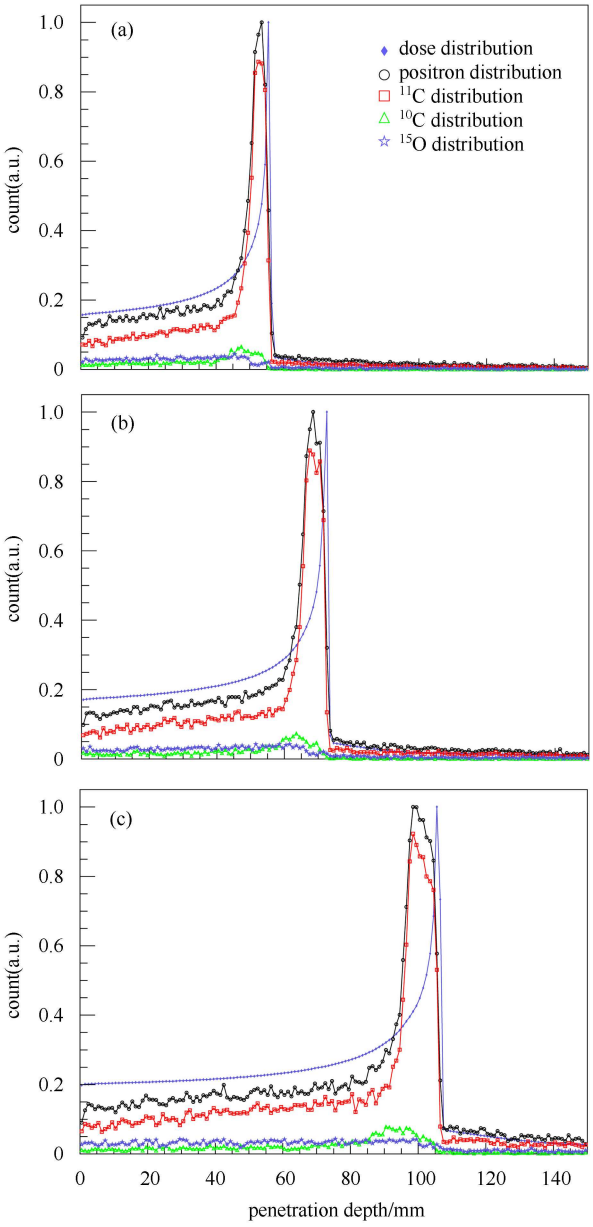

Fig. 5. (color online) Simulated depth distribution of the deposited energy (diamond) and positron activity (circle) for (a) 172, (b) 200, (c) 250 MeV/u ^{12}C nuclei in the PMMA phantom. The distributions of ^{11}C, ^{10}C and ^{15}O are also shown.

Table 2. Calculated yields of positron-emitting nuclei produced by 172, 200 and 250 MeV/u ^{12}C ions.

	172 MeV/u	200 MeV/u	250 MeV/u
^{11}C	6.88 %	8.99 %	12.03 %
^{10}C	0.96 %	1.10 %	1.59 %
^{15}O	1.21 %	1.45 %	2.23 %

distances between 50% distal falloff of Bragg peak and that of the positron activity peak are 1.2%, 1.4% and 1.0%.

Although the two kinds of peaks do not overlap, there is a correlation of the dose and positron activity falloff at the distal edge [4]. Parodi and Bortfeld [6] demonstrated a feasibility of dose recovery from the positron distribution, which indicates the possibility of using PET to monitor carbon beam therapy.

3.3 PET images

We use the 3D MLEM algorithm to reconstruct the activity distribution images for the three kinds of PET scanner, and use ROOT software to analyze the images. In order to compare the performance of the scanners, the longitudinal profiles of reconstructed images, positron activity distribution and dose distribution are shown together in Fig. 6.

The location of 172, 200 and 250 MeV/u carbon beam was on the left, in the center and on the right of the FOV, respectively. In all three cases, there is no significant difference between the image obtained by the dual-plate, four-head and full-ring scanners. Consequently, it is feasible to use the dual-plate PET scanner to monitor the dose distribution for carbon ion therapy.

4 Discussion and conclusions

We proposed dual-plate scanners for dose verification in carbon ion therapy. In the simulation study, the dual-plate scanner avoids interference with the beamline, and the feasibility of using such a scanner to monitor the dose distribution is shown. The image performance of the dual-plate is worse than that of the four-head and full-ring scanner, however, especially at the periphery of the FOV, which is due to the planar nature of the data.

Due to the relative low sensitivity of dual-plate PET, within the limited acquisition time (around 5 mins [4]), the system can only have low statistical data, which will blur the reconstructed image. Usually, we place the irradiated tissue in the middle of the system, which has higher sensitivity, to get more data. We also use the the middle slice of the reconstructed image, which has good spatial resolution, to determine the depth of the Bragg peak. The dual-plate PET is therefore still capable of making this measurement.

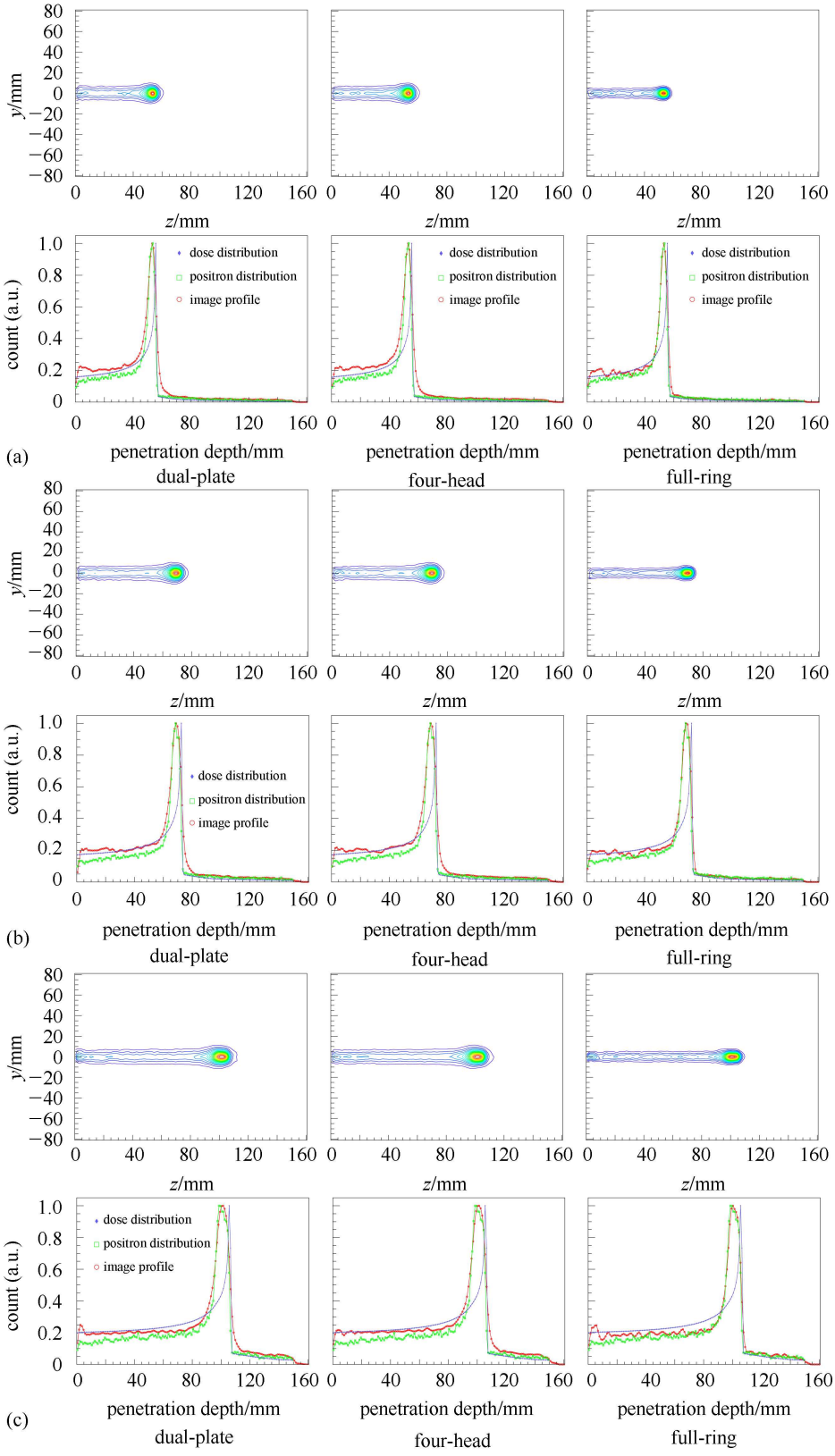

Fig. 6. (color online) The reconstructed PET images and their longitudinal profiles for (a) 172; (b) 200; (c) 250 MeV/u ^{12}C nuclei in the PMMA phantom. The simulated dose and β^+ activity distributions are also shown for comparison.

The gap between the Bragg peak and the profile of the reconstructed image is caused by the different physical processes that the dose distribution and the produced distribution of positron emitters undergo. So, it is not possible to directly evaluate the dose distribution using the reconstructed image. There does exist a correlation of the dose and positron activity falloff at the distal edge, however. By using a special filter function for phantoms in one dimension within the area of the distal falloff of the dose, the dose distribution can be recovered from the positron activity distribution [6].

With the dual-plate scanner, the maximum yield position of positron emitters has been successfully measured, and the longitudinal profiles of reconstructed images and positron activity distribution match well.

In conclusion, the results of this simulation indicate that using a dual-plate PET scanner to monitor carbon ion therapy is feasible.

References

1 Enghardt W, Crespo P, Fiedler F, Hinz R, Parodi K, Pawelke J, P nisch F. Nuclear Instruments and Methods in Physics Research Section A: Accelerators, Spectrometers, Detectors and Associated Equipment, 2004, **525**: 284–288

2 Pshenichnov I, Mishustin I, Greiner W. Physics in Medicine and Biology, 2006, **51**: 6099

3 Lazzeroni M, Brahme A. Physics in Medicine and Biology, 2011, **56**: 1585

4 Shakirin G, Braess H, Fiedler F, Kunath D, Laube K, Parodi K, Priegnitz M, Enghardt W. Phys. Med. Biol., 2011, **56**: 1281

5 Jan S, Benoit D, Becheva E, Carlier T, Cassol F, Descourt P, Frisson T, Grevillot L, Guigues L, Maigne L, Morel C, Perrot Y, Rehfeld N, Sarrut D, Schaart D R, Stute S, Pietrzyk U, Visvikis D, Zahra N, Buvat I. Physics in Medicine and Biology, 2011, **56**: 881

6 Parodi K, Bortfeld T. Physics in Medicine and Biology, 2006, **51**: 1991